Impact-resistance mechanism of gradient ceramic/high entropy alloy composite structure

Wenrui Wang, Wei Ye, Kuisong Huang, Lu Xie, Qing Peng, Fei Zhao & Hanlin Li

Published online: 26 Jul 2023.

Submit your article to this journal ☞

Article views: 206

View related articles ☞

View Crossmark data ☞

Taylor & Francis
Taylor & Francis Group

Check for updates

RESEARCH ARTICLE

Impact-resistance mechanism of gradient ceramic/high entropy alloy composite structure

Wenrui Wang[a,b], Wei Ye[a] (iD), Kuisong Huang[a], Lu Xie[a], Qing Peng[c], Fei Zhao[d], and Hanlin Li[e]

[a]School of Mechanical Engineering, University of Science and Technology Beijing, Beijing, China; [b]The Key Laboratory of Fluid and Matter Interaction, University of Science and Technology Beijing, Beijing, China; [c]State Key Laboratory of Nonlinear Mechanics, Institute of Mechanics, Chinese Academy of Sciences, Beijing, China; [d]National Center for Materials Service Safety, University of Science and Technology Beijing, Beijing, China; [e]School of Design and Creative Arts, Loughborough University, Loughborough, UK

ABSTRACT

The gradient ceramic/high-entropy alloy (HEA) composite combines the high hardness of ceramics and the high toughness of metal alloys with a gradient spacious distribution. It is designed to improve the penetration resistance as a promising protective material with high specific stiffness and strength. In this work, the equivalent model of gradient ceramic/HEA composite material is established by adopting layered structure design, and the material properties of gradient material with different ceramic volume content are calculated. Combined with stress wave theory and numerical simulation of the separated Hopkinson pressure bar, the stress wave propagation under impact is studied for the gradient ceramic/HEA composite and the ceramic/HEA double-layered material. The anti-penetration mechanism is scrutinized. The interlaminar wave impedance increase gradually in the gradient composite but smaller than in double-layered material. The coefficient of reflected stress wave in the gradient composite is much smaller than that of the double-layered material. With the increment of ceramic volume content, the reflected wave amplitude in the gradient composites gingerly decreases. Opposed to the distinct interlayer interfaces that discontinue stress waves in the double-layered material, the internal interface of the gradient composite is much more tranquil and modulate the stress wave smoothly and synchronically with the gradient of composite. The smoothened internal interface is the key and the mechanism the better impact resistance of the gradient material. Our results might be beneficial in material design of the protective materials for impact resistance.

1. Introduction

The most important features of modern warfare are mobility and speed [1,2]. Armored vehicles demand good anti-penetration capabilities and ensure the lightweight to improve mobility [3]. Although the traditional ceramic-metal double-layered armor meets the requirements of lightweight [4–6], there is a sudden change in elastic modulus, hardness, and density between the ceramic faceplate and the metal backplate, and the stress wave propagation of this armor structure has a strong damage to the interior of the structure when it is impacted, reducing its impact resistance [7,8]. It is an urgent problem to reduce the secondary damage caused by stress waves to materials.

Compared with laminated composite materials, gradient composite materials have made great improvements in structure, and the contents of ceramics and metals show a continuous transition change along the thickness direction, which greatly alleviates the stress concentration at the interface of the material and enhances the impact resistance of the material [9–11]. Zhao et al. [12] studied the dynamic response of clamped square sandwich panels with layered-gradient closed-cell aluminum foam cores under the impact

of metallic foam projectiles. The results show that all the sandwich panels have a better shock resistance performance than the same quality single solid plates. The use of layered gradient core can promote the energy absorption of sandwich panels and improve the impact resistance. Zhong et al. [13] designed two types of quasi-continuous TiB/Ti armor with 16 sequential gradient layers, and the functionally graded armor possesses excellent anti-penetration performance and secondary strike ability by optimizing the acoustic impedance matching as revealed by the ballistic test. Sharma et al. [14] fabricated boron carbide reinforced Al–Zn–Mg–Cu matrix FGM by hot pressure-assisted sintering. ballistic tests shown that the high frictional resistance offered by the presence of the ceramic rich layers have resulted in its better ballistic performance. Huang et al. [15,16] used powder metallurgy method make the functionally graded Al_2O_3–ZrO_2 composite. ballistic tests shown that FGM had the best impact resistant performance. Through SEM observation, delamination was not found in the interlayer of FGM, which reduced the tensile wave occurred in the interface between layers and delayed the crack propagation, resulting in a higher ballistic resistance capability structure. Gunes et al.

[17] investigated the damage conditions of the functionally graded plates composed of metal-rich ($n = 0.1$), linear ($n = 1.0$) and ceramic-rich ($n = 10.0$) material compositions under different projectile impact angles. It is found that the material composition gradient and projectile impact angle have significant effects on the ballistic performance of the plates. When the $n = 0.1$ is changed to $n = 10.0$, the ballistic limit value increases by 25% when the ratio of the impact angle changes from 0° to 45°. In summary, different gradient structures and component distributions have a greater impact on the impact resistance of materials. However, the propagation mechanism of stress waves in gradient composites has not been discussed deeply enough. Therefore, clarifying the propagation form of stress waves is helpful to guide the structural design of gradient composites, reduce the propagation intensity of internal stress waves, and improve the impact resistance.

In addition to the structural design of gradient composite materials, the choice of gradient material itself is equally important. Recently there has been a new emerging kind of material known as High-entropy alloys (HEA) [18]. This kind of alloy alters the types and proportions of elements in the alloy to achieve higher strength [19,20], plasticity [21,22], and high temperature softening resistance [23]. Hence, HEAs also have promising applications in armor protection [24,25]. Muskeri et al. [26] evaluated the ballistic response of spherical E52100 steel (RC60) projectiles to a single-phase Al0.1CoCrFeNi high-entropy alloy at a velocity ranging from 500 to 1000 m·s − 1 at normal obliquity. The ballistic results show that the material failure is caused by the growth of ductile pores. Geantă et al. [27] tested the impact resistance of four high-entropy alloy samples with different chemical compositions. The results show that the $AlCrFeCoNi_{1.8}$ material has the best anti-missile characteristics, and it resisted the penetration of two rounds of 7.62 mm armor-piercing incentores. Wang et al. [28,29] studied the effect of ceramic particle distribution on the penetration resistance of materials and prepared TiC-TiB_2/75 vol%$Al_{0.3}CoCrFeNi$ gradient composite by ultra-high gravity field combustion synthesis. For the same ceramic volume fraction, the penetration resistance of gradient composites is better than that of ceramic-metal sandwich composites.

At present, the research on gradient composite mainly focuses on the material's structure design and associated preparation method, and the ballistic performance of materials is tested through impact experiments, but the research on the propagation and action mechanism of stress waves in the materials is still limited. Therefore, it is necessary to conduct a systematic study of the impact of the gradient composite to clarify the mechanism of impact damage. This paper establishes the equivalent model of gradient composite materials, and studies the effect of wave impedance on the impact resistance behavior of ceramic/HEA double-layered material and gradient ceramic/HEA composite using the theoretical method. The propagation law of stress waves in two different materials is compared. Meanwhile, the impact resistance of ceramic/HEA single-layered material, double-layered material and gradient composites with different ceramic volume content are studied by separated Hopkinson pressure bar (SHPB) simulation. Finally, the impact resistance mechanism of gradient composites is deeply analyzed.

2. Theoretical and numerical models

2.1. Propagation law of stress waves in layered materials

When the double-layer composite is impacted, the generated stress wave propagates in two different media, reflecting and transmitting at the interface. The strength and properties of the wave are determined by the material wave impedance [30–33]. Besides the case where the stress wave is incident vertically, the other propagation directions maintain a certain inclination angle with the layer interface. Figure 1(a) shows the propagation paths of stress waves in two materials with mismatched impedances, where θ_1 is the incident angle and reflection angle, and θ_2 is the transmission angle.

We assume the longitudinal wave velocities of the stress wave propagating in material A and material B are C_1 and C_2, respectively. The corresponding wave impedances of these two materials are $\rho_1 C_1$ and $\rho_2 C_2$, respectively. Since the two materials are always in contact, the particles on both sides of the interface follow the continuity condition. Then the relationship between the particle velocities on both sides of the interface can be obtained:

$$v_i + v_r = v_t \tag{1}$$

According to Newton's third law, the stress on both sides of the interface satisfies the equilibrium relationship:

$$\sigma_i + \sigma_r = \sigma_t \tag{2}$$

In Eqs. (1) and (2), v_i, v_r, v_t are the particle velocities on the moving paths of the incident wave, the reflected wave and the transmitted wave, respectively, and $\sigma_i, \sigma_r, \sigma_t$ are the intensities of the incident wave, the reflected wave and the transmitted wave, respectively.

According to the conservation of wavefront momentum, the relationship between stress and particle velocity is satisfied [34]: $\sigma = (\rho C)v$, then:

$$\frac{\sigma_i}{\rho_1 C_1} - \frac{\sigma_r}{\rho_1 C_1} = \frac{\sigma_t}{\rho_2 C_2} \tag{3}$$

Combining Eqs. (1), (2) and (3), the following relationship can be obtained:

$$\begin{cases} \sigma_r = \dfrac{\rho_2 C_2 - \rho_1 C_1}{\rho_2 C_2 + \rho_1 C_1} \sigma_i = R\sigma_i \\ \sigma_t = \dfrac{2\rho_2 C_2}{\rho_2 C_2 + \rho_1 C_1} \sigma_i = T\sigma_i \end{cases} \tag{4}$$

$$\begin{cases} v_r = -\dfrac{\rho_2 C_2 - \rho_1 C_1}{\rho_2 C_2 + \rho_1 C_1} v_i = -Rv_i \\ v_t = \dfrac{2\rho_2 C_2}{\rho_2 C_2 + \rho_1 C_1} v_i = Tv_i \end{cases} \tag{5}$$

In Eqs. (4) and (5), R and T represent the reflection coefficient and transmission coefficient of the double-layered
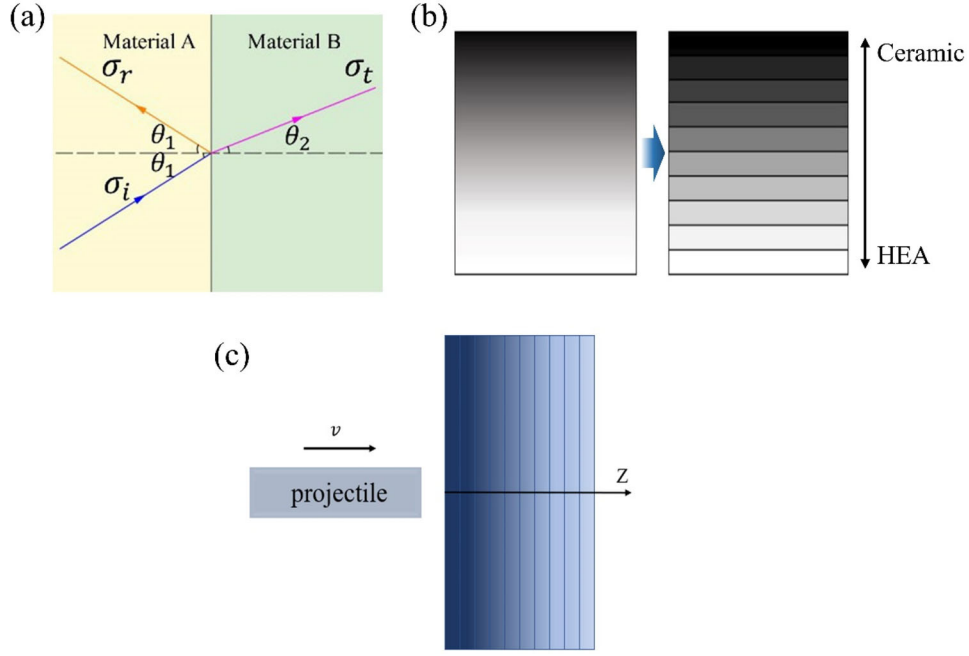
Figure 1. (a) Reflection and refraction of stress waves in a double-layered material; (b) schematic diagram of the structural design of the gradient composite; (c) the layered model of gradient ceramics/HEA material.

structure, respectively. With the wave impedance ratio $\lambda = \rho_1 C_{1/\rho_2} C_2$, one can obtain:

$$\begin{cases} R = \dfrac{\rho_2 C_2 - \rho_1 C_1}{\rho_2 C_2 + \rho_1 C_1} = \dfrac{1 - \lambda}{1 + \lambda} \\ T = \dfrac{2\rho_2 C_2}{\rho_2 C_2 + \rho_1 C_1} = \dfrac{2}{1 + \lambda} \end{cases} \quad (6)$$

2.2. Material characteristics and constitutional model of gradient composite

In the gradient ceramic/HEA composite, the volume fraction of the ceramic phase changes continuously along the thickness direction of the target plate. Therefore, it is macroscopically inhomogeneous and anisotropic [11]. To establish the analytical model of the gradient structure, the gradient composite is divided into several layers along the thickness direction using an equivalent substitution method. When the thickness of each layer is extraordinarily small, it can be approximately considered that the ceramic and metal in each layer are homogeneously mixed. With this approximation, the constituents and properties are the uniform in one layer. The layered model of the gradient ceramic/HEA composite is shown in Figure 1(b).

Metal matrix composites reinforced with ceramic particles can be considered elastic/viscoplastic materials. The stress-strain relationship of the mixed material can be expressed as [35,36]:

$$\sigma(f, \varepsilon, \dot{\varepsilon}) = \sigma_0(\varepsilon) g(V_c) \left[1 + \left(\dfrac{\dot{\varepsilon}}{\dot{\varepsilon}_0} \right)^m \right] \left[1 + \left(\dfrac{\dot{\varepsilon}}{\dot{\varepsilon}_0} \right)^m V_c \right] \quad (7)$$

In Eq. (7), $\sigma_0(\varepsilon)$ represents the stress-strain response of the matrix material under quasi-static conditions. The Parameters

m and $\dot{\varepsilon}_0$ determine the strain rate dependence of the matrix material. The last term in Eq. (7) represents the direct coupling of the strain-rate and volume fraction effects. $g(V_c)$ represents the change of the yield stress with the volume content V_c of the reinforcing phase under quasi-static conditions, and it can be expressed as [35]:

$$g(V_c) = 1 + 1.17 V_c + 2.28 V_c^2 + 21 V_c^3 \quad (8)$$

The work hardening of the matrix is incorporated within $\sigma_0(\varepsilon)$ and is assumed to be independent of strain rate [35]. Therefore, The yield stress σ_s of the composites under quasi-static conditions can be expressed as:

$$\sigma_s = \sigma_0(\varepsilon)(1 + 1.17 V_c + 2.28 V_c^2 + 21 V_c^3) \quad (9)$$

Gradient ceramic/HEA composites are composed of ceramics and high-entropy alloys. They also belong particle-reinforced composite materials. The viscoplastic properties of the materials can be obtained from Eq. (9). The material properties of gradient ceramic/HEA composites can be determined using Mori-Tanaka meso-mechanical method [37–40]. The local effective bulk modulus K and shear modulus G of the gradient composite is estimated by the M-T method as expressed as follows:

$$\begin{cases} \dfrac{K - K_m}{K_c - K_m} = \dfrac{V_c}{\left[1 + (1 - V_c) \frac{3(K_c - K_m)}{3K_m + 4G_m} \right]} \\ \dfrac{G - G_m}{G_c - G_m} = \dfrac{V_c}{\left[1 + (1 - V_c) \frac{G_c - G_m}{G_m + f} \right]} \\ f = \dfrac{G_m(9K_m + 8G_m)}{6(K_m + 2G_m)} \end{cases} \quad (10)$$

where K_m and K_c are the bulk modulus of the matrix and the reinforcing phase, respectively; G_m and G_c are the shear

modulus of the matrix and the reinforcing phase, respectively.

The elastic modulus E and Poisson's ratio ν of each layer of the gradient composite can be calculated from the bulk modulus K and shear modulus G as follows:

$$\begin{cases} G = E/2(1+\nu) \\ K = E/3(1-2\nu) \end{cases} \tag{11}$$

The density ρ of the composite material can be expressed as:

$$\rho = \rho_m(1-V_c) + \rho_c V_c \tag{12}$$

where ρ_m and ρ_c are the density of the matrix and the reinforcing phase, respectively.

In the numerical simulation calculation, the unit failure method is introduced and the failure strain (FS) of the HEA matrix is taken as 2.0. When the failure strain reaches 2.0, the unit of the HEA is removed. The failure strain ε_f of the composite can be expressed as [41]:

$$\varepsilon_f = \varepsilon_{f0}/(1 + 1.17V_c + 2.28V_c^2 + 21V_c^3) \tag{13}$$

where ε_{f0} is the FS of the metal-matrix.

According to the material parameters of the high-entropy alloy matrix and the ceramic reinforcing phase in Table 1, the density, elastic modulus, Poisson's ratio, yield stress, and other gradient ceramic/HEA composite parameters can then be obtained.

The mechanical response of the gradient ceramic/HEA composite is simulated using the Plastic-Kinematic model (P-K model), which considers the isotropic and kinematic hardening model of the strain rate effect [29]. The isotropic or kinematic hardening can be selected by adjusting the hardening parameters β ($0<\beta<1$) [43]. In the LS-DYNA handbook, the P-K model is combined with the Cowper-Symonds model to consider the strain rate effect of the material [44]:

$$\begin{cases} \sigma_y = \left[1 + \left(\frac{\dot{\varepsilon}}{C}\right)^{\frac{1}{P}}\right](\sigma_0 + \beta E_p \varepsilon_{eff}^p) \\ E_p = \dfrac{E_t - E}{E - E_t} \end{cases} \tag{14}$$

where C and P are the dimensionless strain rate parameters; $\dot{\varepsilon}$ is the strain rate; σ_0 is the yield stress of the material under quasi-static conditions; ε_{eff}^p is the effective plastic deformation; E_p is the plastic hardening modulus; and E_t is the tangent modulus.

2.3. SHPB numerical simulation

The separated Hopkinson pressure rod technique (SHPB) is commonly used to study the dynamic mechanical property of engineering materials. The complete stress wave information can be recorded by Hopkinson bar during the impact process, so it is very suitable for the study of impact damage mechanism.

SHPB simulation analysis was performed using ANSYS/LS-DYNA explicit analysis software. Since the computational model and the boundary are symmetrical, a 1/4 model is established to reduce the computation demands. The schematic diagram of the SHPB model, the one-quarter SHPB finite element model and the sectional grid diagram are shown in Figure 2. The three-dimensional Solid164 element is used to mesh the model. The total number of meshes in the finite element model is 190170 and the number of elements on the axis of the specimen is 30. The system's initial condition is the impact velocity of the impact rod, the pressure rod, and the specimen can move freely in the axial direction. To ensure the integrity of the ceramic material, the initial velocity of the striker rod was set to 15 m/s. The surface-to-surface contact is set between the

Table 1. Model parameters of HEAs and ceramic materials [29,42].

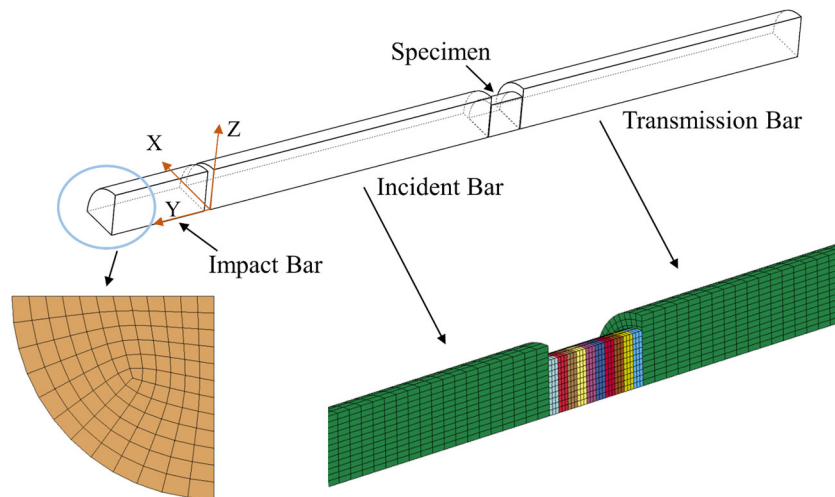| Material	Density/kg.m^{-3}	Elastic Modulus /GPa	Poisson's ratio	Shear modulus /GPa	Yield stress/MPa
Al$_{0.3}$CoCrFeNi	7860	216	0.3	83	216
SiC	3163	435	0.17	183	—

Figure 2. SHPB schematic and finite element model.

pressure rod and the specimen. The material types of the test pieces are shown in Table 2.

The gradient ceramic/HEA composite parameters for three different ceramic volume fractions are shown in Figure 3. The materials of other specimens are all selected with appropriate constitutive models. The SiC ceramic material adopts the Johnson-Holmquist II material model [43]. The high-entropy alloy material adopts the P-K model. The impact rod, incident rod and transmission rod are all elastic steel materials, which are described by the *MAT_ ELASTIC linear elastic material model.

3. Results and discussion

3.1. Theoretical analysis of stress wave propagation in gradient composites

A uniaxial coordinate system is established along the thickness direction of the gradient ceramic/HEA target plate. The z-axis coincides with the central axis of the target plate, and the concentration of SiC ceramic particles continuously change along the thickness direction of the target plate, as shown in Figure 1(c). In the positive direction of the z-axis,

Table 2. Material type of each test piece.

Specimen serial number	Material
Specimen 1	HEA single-layered target
Specimen 2	SiC ceramic single-layered target
Specimen 3	Double-layered target (50%SiC)
Specimen 4	Gradient composite target (10%SiC)
Specimen 5	Gradient composite target (30%SiC)
Specimen 6	Gradient composite target (50%SiC)

the ceramic volume fraction gradually decreases. The distribution law of ceramic volume fraction follows the expression:

$$V_c = a\frac{z}{H} \qquad (0 \leq a \leq 1) \tag{15}$$

In Eq. (15), V_c represents the volume content of ceramics, H represents the total thickness of the target plate, z is the coordinate, and a determines the average volume content of ceramics. The target plate is divided into 10 layers, and the coordinates are set at the middle position of each layer.

The ceramic volume content of each layer is a function of the thickness direction. Combined with Eqs. (9) to (13), the gradient composites with 10%∼50% volume content of five different ceramics are calculated. The distribution law of each parameter can then be obtained, as shown in Figure 3.

When the gradient ceramic/HEA composite is impacted, the stress wave reaches the target plate's back through layer-by-layer transition and reflects on the interfaces [45,46], as shown in Figure 4(a). The stress relationship between material gradient interfaces can be expressed as:

$$\begin{cases} \sigma_1 = T_1\sigma_0, \sigma'_0 = R_1\sigma_0 \\ \sigma_2 = T_2\sigma_1, \sigma'_1 = R_2\sigma_1 \\ \dots \\ \sigma_n = T_n\sigma_{n-1}, \sigma'_{n-1} = R_n\sigma_{n-1} \end{cases} \tag{16}$$

where σ_1, …, σ_n are the transmitted wave intensity of the interlayer transition interface, T_1, T_2, …, T_n are the corresponding transmission coefficients, $\sigma_{1'}$, …, $\sigma_{n-1'}$ are the reflected wave intensity of the interlayer transition interface, R_1, R_2, …, R_n are the corresponding reflection coefficients.
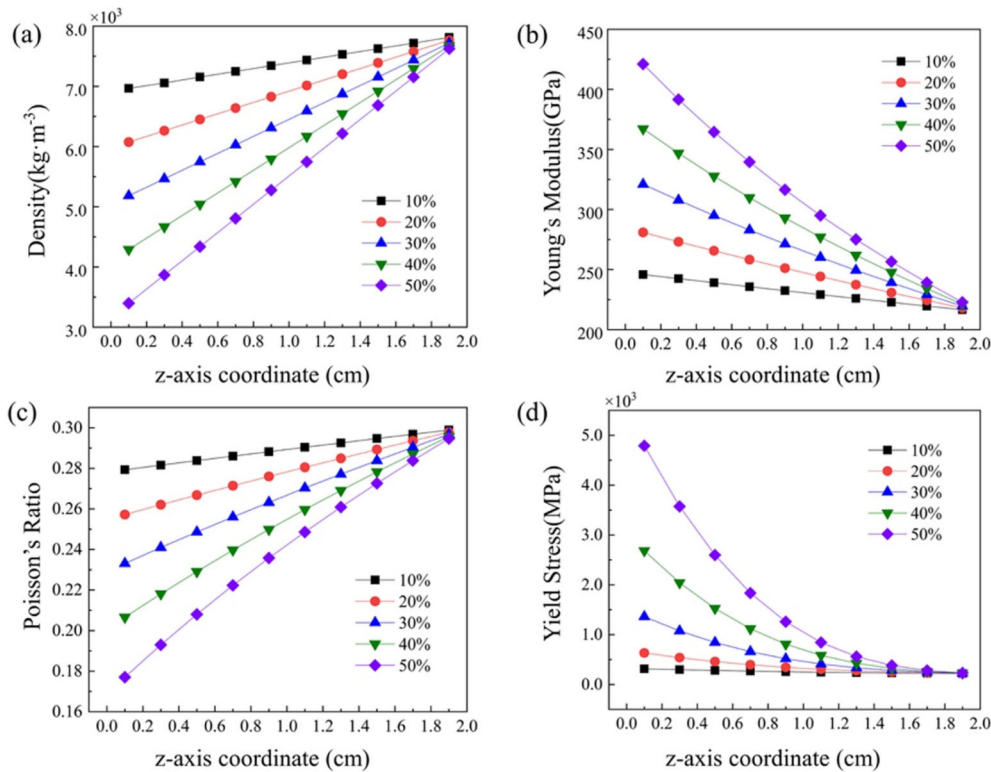

Figure 3. The distribution law of the volume content of ceramics in each layer of the target plate with different ceramic volume contents.
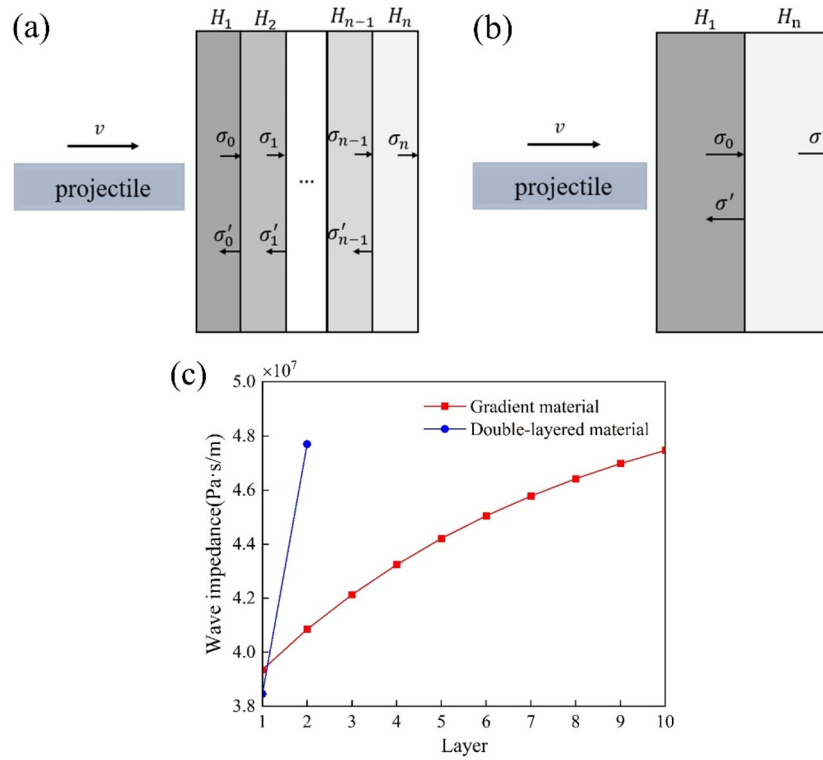
Figure 4. (a) Schematic of stress wave propagation in gradient composites; (b) schematic of stress wave propagation in the double-layered materials; (c) wave impedance on the interfaces of the gradient material as a function of layer number, compared to that of the double-layered material.

According to Eq. (6), the reflection and transmission coefficients within the gradient ceramic/HEA composite can be expressed as:

$$
\begin{cases}
T_1 = \dfrac{2}{1+\lambda_1}, T_2 = \dfrac{2}{1+\lambda_2}, ..., T_n = \dfrac{2}{1+\lambda_n} \\
R_1 = \dfrac{1-\lambda_1}{1+\lambda_1}, R_2 = \dfrac{1-\lambda_2}{1+\lambda_2}, ..., R_n = \dfrac{1-\lambda_n}{1+\lambda_n}
\end{cases}
\tag{17}
$$

where λ_1, λ_2, ..., λ_n are the ratios of the wave impedances between adjacent materials, for example, $\lambda_n = \rho_{n-1}C_{n-1}/\rho_n C_n$. Based on Eq. (17), Eq. (16) is iteratively calculated, and the reflected wave intensity and transmitted wave intensity on the back of the gradient composite can be calculated using the following equations:

$$
\begin{cases}
\sigma_n = \dfrac{2^n \sigma_0}{(1+\lambda_1)} \\
\sigma'_{n-1} = \dfrac{2^{n-1}(1-\lambda_n)\sigma_0}{(1+\lambda_1)(1+\lambda_2)...(1+\lambda_n)}
\end{cases}
\tag{18}
$$

The ceramic/HEA double-layered materials are forced to match together by means of certain measures. Due to the rough machining surface of the ceramic and the significant difference in the thermal expansion coefficients of the ceramic materials and HEA materials, the two materials cannot be seamlessly matched. When the double-layered material is impacted, the stress wave is directly transmitted from the ceramic material into the HEA material, as shown in Figure 4(b).

Then, the transmitted wave intensity σ and reflected wave intensity σ' in the ceramic/HEA double-layered

material can be expressed as:

$$
\begin{cases}
\sigma = \dfrac{2}{1+\lambda}\sigma_0 \\
\sigma' = \dfrac{1-\lambda}{1+\lambda}\sigma_0
\end{cases}
\tag{19}
$$

where λ is the ratio of the wave impedance of the ceramic material and the HEA material, $\lambda = \rho_0 C_0/\rho_n C_n$. C_0 and C_n are the longitudinal wave velocities of stress waves in ceramic materials and high-entropy alloy materials, respectively.

Gradient ceramic/HEA composite and ceramic/HEA double-layered material with a ceramic volume content of 50% were selected, and the wave impedances of the two types of target plates were calculated, as shown in Figure 4(c).

The results showed that the wave impedance inside the gradient ceramic/HEA composite increases gradually. In contrast, the ceramic and HEA wave impedance in the ceramic/HEA double-layered material changes abruptly. According to the value of the wave impedance, the internal reflection coefficient R and transmission coefficient T of the two materials are obtained by Eq. (6), as shown in Tables 3 and 4.

The reflection coefficient of the gradient ceramic/HEA composite is much smaller than that in the ceramic/HEA double-layered material. This means that the wave impedance inside the gradient ceramic/HEA composite is almost matched, which significantly weakens the propagation intensity of the reflected stress wave and reduces the possibility of internal cracks in the material. In addition, the transmission coefficients of each layer of the gradient ceramic/HEA composite are also smaller than the transmission coefficient

between the ceramic/HEA double-layered material. The reduction of the transmitted wave intensity makes the target plate bear less impact stress and obtain better ballistic performance.

The transmission stress and reflection stress of the two materials are obtained from Eqs. (18) and (19), as shown in Table 5. The total transmitted stress of the gradient ceramic/HEA composite is close to that of the ceramic/HEA double-layered material, but the total reflected stress is much smaller than that of the double-layered material. Since the gradient composite is regarded as a material composed of n layers with small thickness and similar properties, the increase of n value makes the intensity of reflected stress wave and transmitted stress wave inside the material smaller. Therefore, the difference between the reflected stress wave

Table 3. The reflection and transmission coefficients between each layer of the gradient ceramic/HEA composite.

(The kth layer, The $(k+1)$th layer)	Reflection coefficient	Transmission coefficient
(1, 2)	0.0186	1.0186
(2, 3)	0.0155	1.0155
(3, 4)	0.0130	1.0130
(4, 5)	0.0110	1.0110
(5, 6)	0.0094	1.0094
(6, 7)	0.0081	1.0081
(7, 8)	0.0069	1.0069
(8, 9)	0.0060	1.0060
(9, 10)	0.0052	1.0052

Table 4. The reflection and transmission coefficients of the interface of ceramic/HEA double-layered material.

(Material A, Material B)	Reflection coefficient	Transmission coefficient
(SiC, CoCrFeNiAl$_{0.3}$)	0.1072	1.1072

Table 5. Transmission stress and reflection stress of two materials.

Material	Transmission stress	Reflected stress
Gradient ceramic/HEA composite	1.0976σ_0	0.0057σ_0
Double-layered ceramic/HEA material	1.1072σ_0	0.1072σ_0

and the transmitted stress wave of the two types of target plates in practical engineering is greater.

3.2. SHPB simulation of stress wave propagation in gradient composites

The propagation of the incident wave reflected wave and transmitted wave of each specimen can be obtained by the SHPB simulation, as shown in Figures 5 and 6. The incident stress amplitude of different specimens is basically unchanged, but the reflected wave and transmitted wave amplitude are obviously different.

Firstly, the stress wave propagation inside the material under single-layered, double-layered and gradient structure is analyzed, as shown in Figure 5. For specimen 1, the amplitude of reflected stress wave is relatively high, and the amplitude of transmitted stress wave is relatively low, and the fluctuation range of reflected stress wave and transmitted stress wave at different times is small. This is because the high-entropy alloy material has strong plasticity and toughness. When the load impacts one end at a low strain rate, elastic deformation will occur and the effect of stress smoothing will be achieved. At the same time, the transmitted wave energy is effectively attenuated. In contrast, although the reflected stress amplitude of specimen 2 is low, the initial stress fluctuates greatly, and a sudden change occurs, and the transmitted stress wave also reaches the maximum value at this time. Under the interaction of the non-uniform change of tensile stress and compressive stress, it is likely to cause damage and failure of the ceramic materials.

Specimen 3 uses a high-hardness ceramic panel and a high-toughness high-entropy alloy backplane. Compared with specimen 1, the amplitude of the reflected stress wave inside specimen 3 decreases and gradually attenuates, while the transmitted stress wave increases. Different from specimen 2, no significant abrupt change is found in the reflected stress waves inside specimen 3, which is due to the plastic deformation of the high-entropy alloy backplane that absorbs most of the energy. Specimen 6 is a gradient
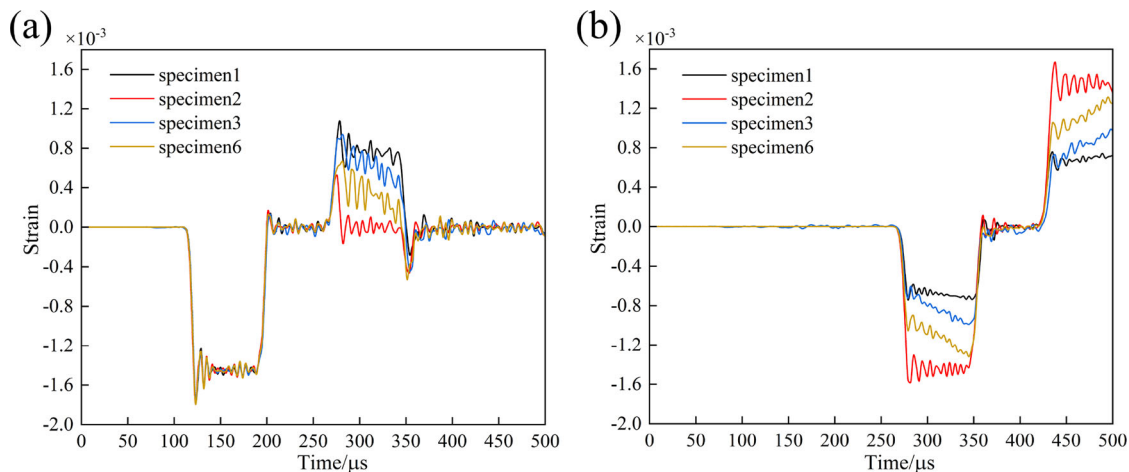

Figure 5. SHPB simulation of stress waves in single-layered, double-layered and gradient structural materials: (a) Incident and reflected waves; (b) transmitted waves.
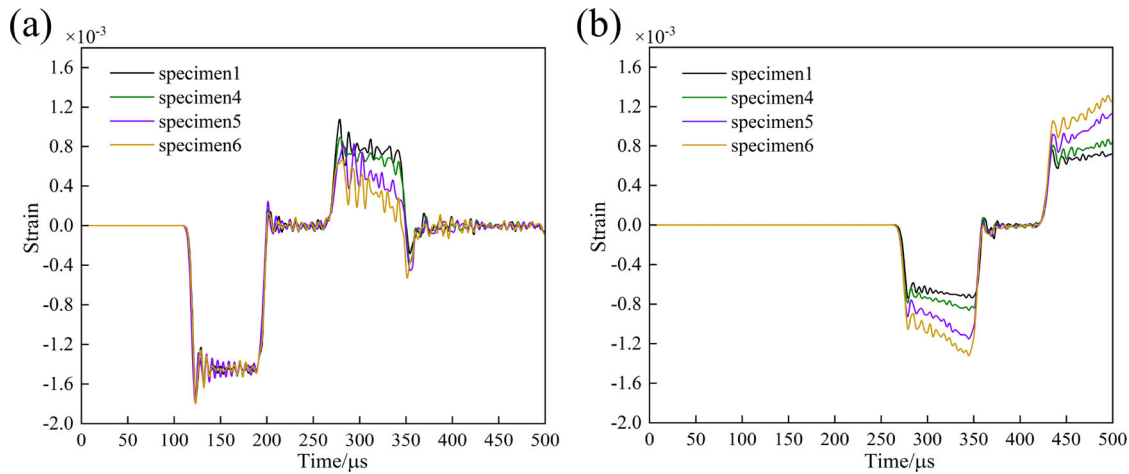
Figure 6. SHPB simulation of stress waves in gradient structural materials with different ceramic volume content: (a) Incident and reflected waves; (b)transmitted waves.

composite structure with the same ceramic volume content as specimen 3. The reflected stress wave amplitude inside the specimen 6 is significantly reduced, and the stress fluctuation range is small, which can effectively reduce the intensity of the reflected stress wave inside the structure, thereby improving the overall impact resistance of the composite material. The amplitude of the transmission stress wave increases and gradually strengthens, because the volume content of the ceramic of the gradient structure gradually decreases along the thickness direction, the plasticity and toughness of the material are gradually enhanced, and the absorption of energy is also gradually enhanced when it is impacted.

In order to study the effect of ceramic volume content on stress wave propagation inside the gradient structure, three gradient composites with different ceramic volume content were compared, as shown in Figure 6. The volume content of ceramic in sample 4 is 10%, and the material still retains high plasticity and toughness, and the amplitude of reflected stress wave and transmitted stress wave is close to that of high entropy alloy single-layer material. With the increase of ceramic volume content, the amplitude of the reflected wave inside the gradient structure decreases obviously and gradually attenuates, while the amplitude of the transmitted wave increases gradually. Therefore, the gradient structure and the distribution of ceramics in the material have a great influence on the propagation of stress waves. The ceramic properties of the front side of the gradient structure are more significant, while the back side still has strong plasticity and toughness, but the volume content of the ceramic is gradually transitive from the front side to the back side, and there is no macroscopic interface inside the structure. Unlike specimen 3, when the ceramic volume content increases to 50%, the reflected stress wave intensity inside the gradient material is still small.

Figure 7 shows the stress distribution cloud diagram along the axial direction of 6 different specimens at 3 different moments. Specimen 1 has a plastic deformation on the whole, and its internal stress distribution is relatively uniform, and the stress changes at different times are basically consistent without sudden change, as shown in Figures 8(a)

and 9(a). The internal stress distribution of specimen 2 is irregular, and it is often a state of coexistence of tensile stress and compressive stress at different times, as shown in Figure 9(b). When the intensity of the stress wave exceeds the fracture criterion of the material, a crack will be generated inside the specimen 2 and be destroyed. The stress distribution in the ceramic panel of specimen 3 is uneven under impact, which is similar to the characteristics of specimen 2. However, when the stress propagates to the high-entropy alloy backplane, the material exhibits obvious plastic deformation. The axial strain suddenly increases, and the internal stress tends to be consistent at different times, as shown in Figures 8(c) and 9(c). The support of the high-entropy alloy backplane absorbs most of the energy for the double-layer material, but the unbalanced wave impedance still inevitably occurs at the interface. When a high-intensity stress wave propagates into the ceramic panel, it will cause large-scale failure of the material.

For gradient composites with different ceramic volume content, the internal stress changes have a certain regularity. The ceramic volume content of specimen 4 is low, and when impacted, it can produce gradient plastic deformation along the thickness direction, absorb most of the energy, and its internal stress is always maintained at a low level, similar to high-entropy alloy single-layered materials, as shown in Figures 8(d) and 9(d). With the gradual increase of the ceramic volume content of the whole gradient material, the strain of specimen 5 and specimen 6 near the panel becomes smaller and smaller, and the energy absorption is gradually weakened, so the stress borne inside the material also gradually increases, as shown in Figures 8 (e,f) and 9(e,f), but the hardness and compressive strength of the gradient composites are also gradually increasing. Compared with the double-layer material, the stress distribution inside the gradient composite material shows a gradient change in Figure 7, rather than disorderly, and the stress changes at different times are small, without sudden change, which effectively reduces the imbalance of the internal wave impedance of the material. The gradient design also enables the energy generated by the impact to be transferred
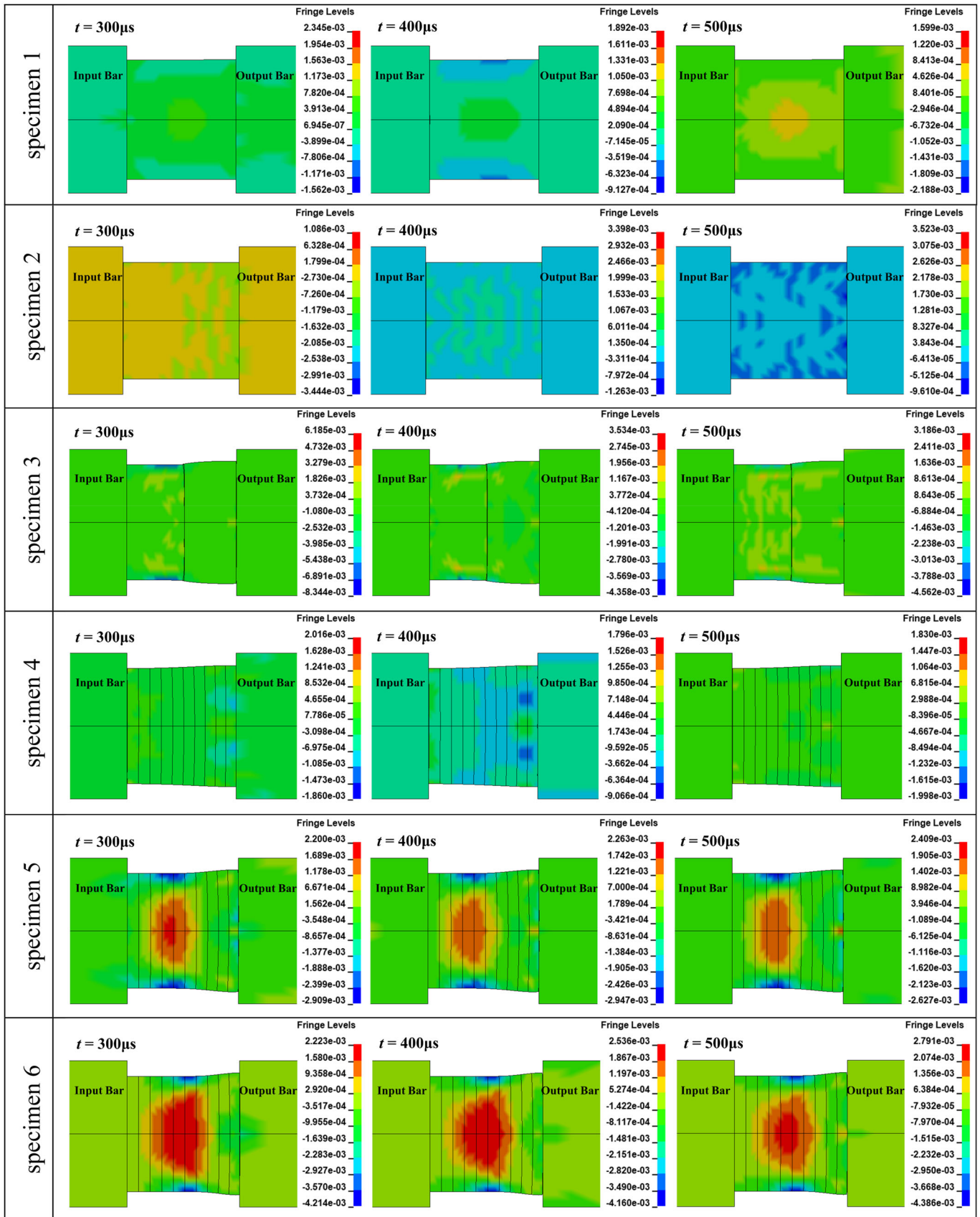
Figure 7. The internal stress axial distribution of each specimen at different moments.

backward step by step, avoiding excessive energy on the side close to the gradient material panel, which prevents the material from being damaged.

Thus, the gradient ceramic/HEA composites can better combine the advantages of ceramics and metals than the double-layered composite. The ceramic materials with low
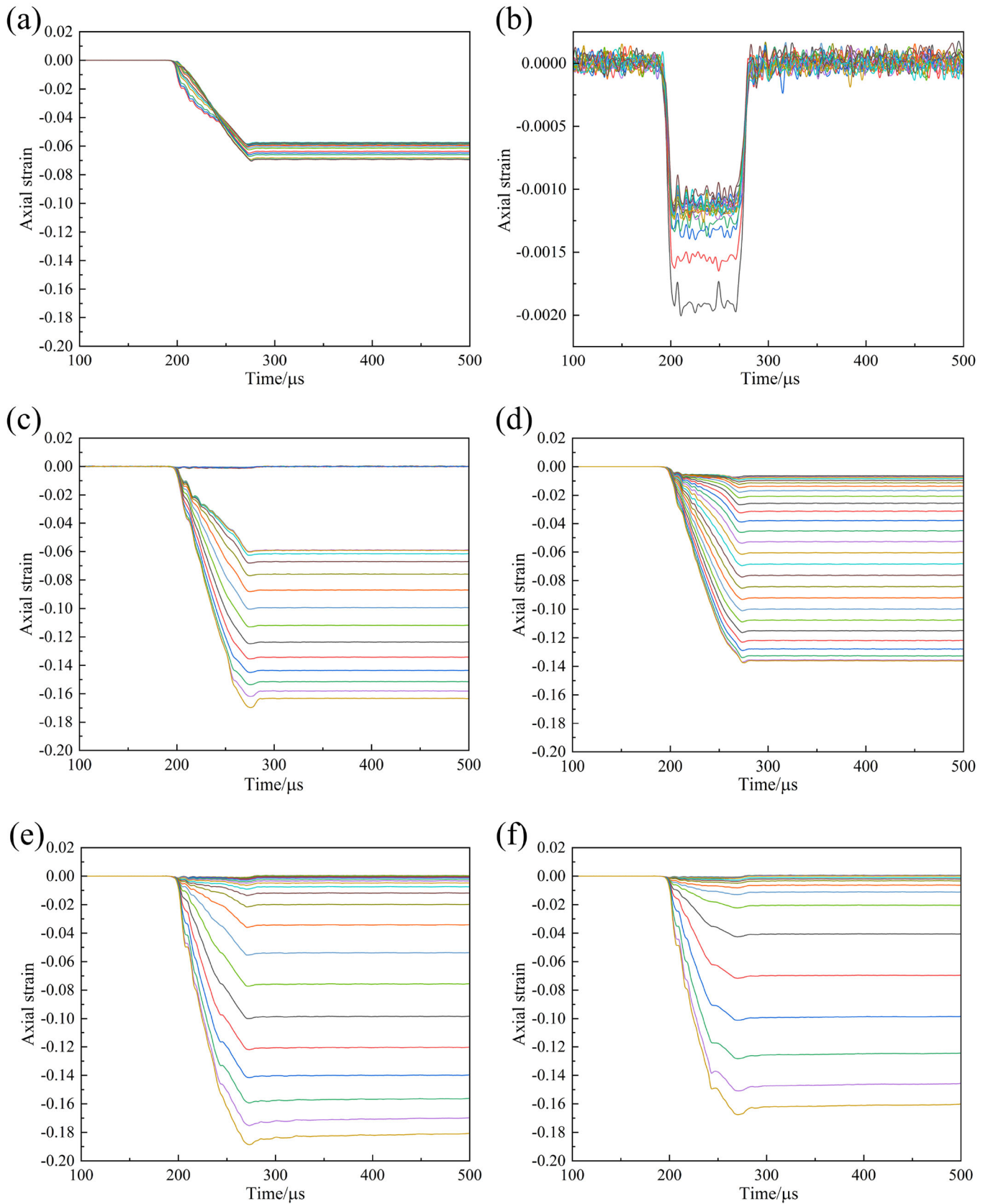
Figure 8. Strain time history curve of the element on the specimen axis: (a) Specimen1; (b) Specimen 2; (c) Specimen 3; (d) Specimen 4; (e) Specimen 5; (f) Specimen 6.

density, high hardness and high compressive strength characteristics can not only reduce the weight of the armor, but also break the projectile body when it is impacted, and improve the anti-penetration ability of the target plate. However, the tensile strength of ceramics is low. According to the results of SHPB simulation, it can be found that the
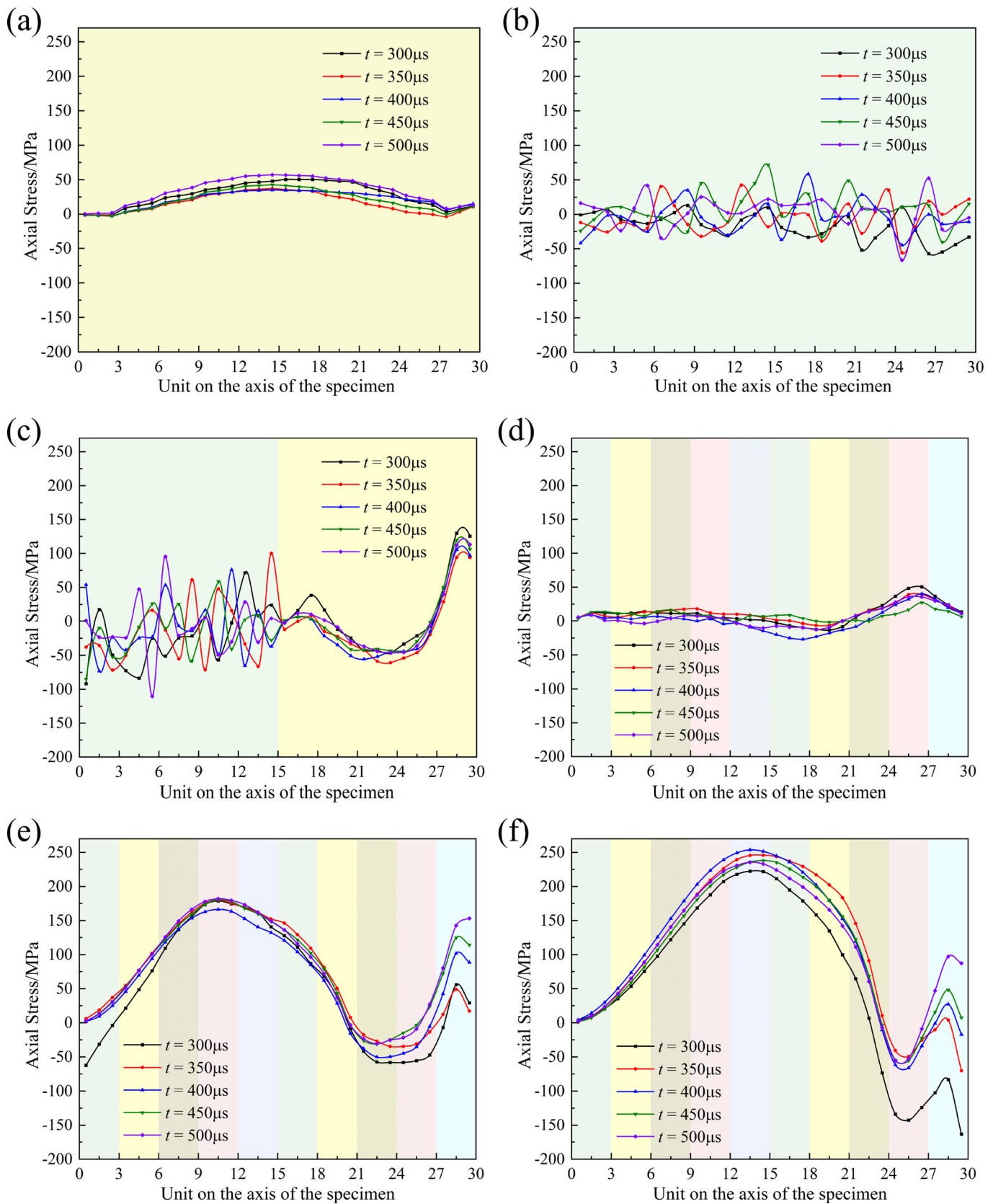
Figure 9. The stress distribution inside the six types of specimens at different moments: (a) Specimen1; (b) Specimen 2; (c) Specimen 3; (d) Specimen 4; (e) Specimen 5; (f) Specimen 6.

reflected stress wave inside the ceramics will change abruptly, and the tensile stress and compressive stress will repeatedly act in the ceramic at different times, which is easy to lead to the failure of ceramic materials. Although the double-layer composites can realize the overall lightweight and provide the support of the metal backplane for the ceramic, it cannot solve the damage of the reflected stress wave to the ceramic material well. Gradient composites can make

better use of the high hardness of ceramics and the high toughness of metals, as well as weaken the damage of stress waves to the overall structure. By rationally designing the ceramic volume content and distribution form inside the gradient composite material, the impact resistance of the gradient composite material can be greatly improved.

4. Conclusion

This paper uses the SHPB numerical simulation method to study the stress wave propagation of gradient ceramic/HEA composites with different ceramic volume content under impact, and compared with ceramic/HEA single-layered materials and double-layered materials. The propagation law of the reflected stress wave and the transmitted stress wave in the gradient ceramic/HEA composite and ceramic/HEA double-layered material is analyzed. The mechanism of the anti-penetration of the gradient composite is discussed. The following conclusions can be drawn: The wave impedance of the gradient composite shows a slowly increasing trend, which avoids the imbalance of the internal wave impedance of the material, and the reflection stress wave is much smaller than that of the double-layered material. Gradient composites' anti-penetration and anti-impact properties are explained in terms of material wave impedance. The volume content of ceramic in the gradient composite greatly influences the overall performance of the material. With the increase of the volume content of ceramic, the amplitude of the reflected wave in the gradient composite gradually decreases, and the amplitude of the transmitted wave gradually increases. The double-layered material has distinct interlayer interfaces, and the wave impedance is seriously unbalanced, which leads to a large change in stress when subjected to impact. On the contrary, the internal interfaces of the gradient composite have much less effect on the wave propagation and stress redistribution. The stress wave shows good coordination and synchronization in the gradient composite, which is an important reason for the better impact resistance of the gradient composite. The smoothened internal interface is the key and the mechanism the better impact resistance of the gradient material. Our numerical investigations might be beneficial in material design of the protective materials with high impact resistance.

Disclosure statement

No potential conflict of interest was reported by the authors.

Funding

ORCID

Wei Ye (iD) http://orcid.org/0000-0003-3137-3312

References

[1] G. Zhang, Y. Liu, Z. Lv, J. Wang, W. Zhang, and Y. Wu, Research on impact resistance of ceramic matrix composites, Compos. Struct., vol. 268, pp. 113977, 2021.

[2] Y. Bao, X. Gao, Y. Wu, M. Sun, and G. Li, Research progress of armor protection materials, J. Phys.: Conf. Ser., vol. 1855, pp. 012035, 2021.

[3] Y.B. Gao, W. Zhang, C.H. Yi, and T. Tang, Effects of adhesive layer on anti-penetration performance of ceramic/metal composite armour, J. Vib. Shock., vol. 38, pp. 95–101, 2019.

[4] S. Sadanandan and J.G. Hetherington, Characterisation of ceramic/steel and ceramic/aluminium armours subjected to oblique impact, Int. J. Impact Eng., vol. 19, no. 9–10, pp. 811–819, 1997. DOI: 10.1016/S0734-743X(97)00019-5.

[5] M. Übeyli, R.O. Yıldırım, and B. Ögel, Investigation on the ballistic behavior of Al2O3/Al2024 laminated composites, J. Mater. Process. Tech., vol. 196, no. 1–3, pp. 356–364, 2008. DOI: 10.1016/j.jmatprotec.2007.05.050.

[6] S. Rathod, G. Tiwari, and D. Chougale, Ballistic performance of ceramic–metal composite structures, Mater Today., vol. 41, pp. 1125–1129, 2021. DOI: 10.1016/j.matpr.2020.08.759.

[7] A. Tasdemirci and I.W. Hall, The effects of plastic deformation on stress wave propagation in multi-layer materials, Int. J. Impact Eng., vol. 34, no. 11, pp. 1797–1813, 2007. DOI: 10.1016/j.ijimpeng.2006.10.005.

[8] X. Wang, M. Yuan, Y. Miao, and Z. Wei, Stress wave propagation characteristics and impact resistance of laminated composites under impact loading, Mech. Adv. Mater. Struct., pp. 1–10, 2022. DOI: 10.1080/15376494.2022.2143602.

[9] Y.W. Wang, F.C. Wang, X.D. Yu, and Z. Ma, Research advancement on graded ceramic-metal armor composites, Acta Armamentarii., vol. 28, pp. 209–214, 2007.

[10] E.S.C. Chin, Army focused research team on functionally graded armor composites, Mater. Sci. Eng. A., vol. 259, no. 2, pp. 155–161, 1999. DOI: 10.1016/S0921-5093(98)00883-1.

[11] V. Bhavar, P. Kattire, S. Thakare, S. Patil, and RKP Singh, A review on functionally gradient materials (FGMs) and their applications, IOP Conf. Ser.: Mater. Sci. Eng., vol. 229, pp. 012021, 2017.

[12] Z. Zhao and L. Jing, The response of clamped sandwich panels with layered-gradient aluminum foam cores to foam projectile impact, Mech. Adv. Mater. Struct., vol. 27, no. 9, pp. 744–753, 2020. DOI: 10.1080/15376494.2018.1495790.

[13] Z. Zhong, B. Zhang, Y. Jin, H. Zhang, Y. Wang, J. Ye, Q. Liu, Z. Hou, Z. Zhang, and F. Ye, Design and anti-penetration performance of TiB/Ti system functionally graded material armor fabricated by SPS combined with tape casting, Ceram. Int., vol. 46, no. 18, pp. 28244–28249, 2020. DOI: 10.1016/j.ceramint.2020.07.325.

[14] A. Sharma, S.S. Kv, M. Dixit, A.K. Gupta, and R. Sujith, Ballistic performance of functionally graded boron carbide reinforced Al–Zn–Mg–Cu alloy, J. Mater. Res. Technol., vol. 18, pp. 4042–4059, 2022. DOI: 10.1016/j.jmrt.2022.04.059.

[15] C.Y. Huang and Y.L. Chen, Design and impact resistant analysis of functionally graded Al2O3–ZrO2 ceramic composite, Mater. Des., vol. 91, pp. 294–305, 2016. DOI: 10.1016/j.matdes.2015.11.091.

[16] C.Y. Huang and Y.L. Chen, Effect of mechanical properties on the ballistic resistance capability of Al2O3-ZrO2 functionally graded materials, Ceram. Int., vol. 42, no. 11, pp. 12946–12955, 2016. DOI: 10.1016/j.ceramint.2016.05.067.

[17] R. Gunes, M. Hakan, M.K. Apalak, and J.N. Reddy, Numerical investigation on normal and oblique ballistic impact behavior of functionally graded plates, Mech. Adv. Mater. Struct., vol. 28, no. 20, pp. 2114–2130, 2021. DOI: 10.1080/15376494.2020.1717023.

[18] J.W. Yeh, S.K. Chen, S.J. Lin, J.Y. Gan, T.S. Chin, T.T. Shun, C.H. Tsau, and S.Y. Chang, Nanostructured high-entropy alloys with multiple principal elements: Novel alloy design concepts

and outcomes, Adv. Eng. Mater., vol. 6, no. 5, pp. 299–303, 2004. DOI: 10.1002/adem.200300567.

[19] T. Xiong, S. Zheng, J. Pang, and X. Ma, High-strength and high-ductility AlCoCrFeNi2.1 eutectic high-entropy alloy achieved via precipitation strengthening in a heterogeneous structure, Scr. Mater., vol. 186, pp. 336–340, 2020.

[20] W. Qi, W. Wang, X. Yang, L. Xie, J. Zhang, D. Li, and Y. Zhang, Effect of Zr on phase separation, mechanical and corrosion behavior of heterogeneous CoCrFeNiZrx high-entropy alloy, J. Mater. Sci. Technol., vol. 109, pp. 76–85, 2022. DOI: 10.1016/j.jmst.2021.08.062.

[21] W. Wang, Y. Lu, Z. Li, and H. Li, Simulations of engine knock flow field and wave-induced fatigue of a downsized gasoline engine, Int. J. Engine Res., vol. 22, no. 2, pp. 554–568, 2021. DOI: 10.1177/1468087419859791.

[22] W.R. Wang, W.L. Wang, S.C. Wang, Y.C. Tsai, C.H. Lai, and J.W. Yeh, Effects of Al addition on the microstructure and mechanical property of AlxCoCrFeNi high-entropy alloys, Intermetallics., vol. 26, pp. 44–51, 2012. DOI: 10.1016/j.intermet.2012.03.005.

[23] A. Gali and E.P. George, Tensile properties of high- and medium-entropy alloys, Intermetallics., vol. 39, pp. 74–78, 2013. DOI: 10.1016/j.intermet.2013.03.018.

[24] Chen Hai-Hua, Zhang Xian-Feng, Liu Chuang, K. Lin, and W. Xiong, Research progress on impact deformation behavior of high-entropy alloys, Explos. Shock Waves., vol. 41, pp. 041402, 2021.

[25] T. Chereches, P. Lixandru, V. Geantă, I. Voiculescu, D. Dragnea, and R. Stefanoiu, Layered structures analysis, with high entropy alloys, for ballistic protection, Appl. Mech. Mater., vol. 809, pp. 724–729, 2015.

[26] S. Muskeri, D. Choudhuri, P.A. Jannotti, B.E. Schuster, J.T. Lloyd, R.S. Mishra, and S. Mukherjee, Ballistic impact response of Al0.1CoCrFeNi high-entropy alloy, Adv. Eng. Mater., vol. 22, no. 6, pp. 2000124, 2020. DOI: 10.1002/adem.202000124.

[27] V. Geantă, I. Voiculescu, R. Stefănoiu, T. Chereches, T. Zecheru, L. Matache, and A. Rotariu, Dynamic impact behaviour of high entropy alloys used in the military domain, IOP Conf. Ser.: Mater. Sci. Eng., vol. 374, pp. 012041, 2018.

[28] W. Wang, H. Xie, L. Xie, X. Yang, J. Li, and Q. Peng, Fabrication of ceramics/high-entropy alloys gradient composites by combustion synthesis in ultra-high gravity field, Mater. Lett., vol. 233, pp. 4–7, 2018.

[29] W.-R. Wang, H.-F. Xie, L. Xie, H. Li, X. Yang, and Y. Shen, Anti-penetration performance of high entropy alloy–ceramic gradient composites, Int. J. Miner. Metall. Mater., vol. 25, no. 11, pp. 1320–1328, 2018. DOI: 10.1007/s12613-018-1685-5.

[30] X. Xu, L. Jin, S.L. Huang, S.Q. Gao, and H. Zhang, Transmission characteristics of impact load of flying debris at epoxy resin/printed circuit board/epoxy resin interfaces, Acta Armamentarii., vol. 41, pp. 1817, 2020.

[31] Q. Zhong, H.L. Hou, X. Zhu, and D. Li, Numerical analysis of penetration resistance of ceramic/fluid cabin composite structure, Explos. Shock Waves., vol. 37, pp. 510–519, 2017.

[32] Y.C. Zou, C. Xiong, J.H. Yin, K. Cui, and H, Deng, Anti-penetration performance experiment and numerical simulation on layered composite structure, Acta Mater. Compositae Sin., vol. 39, pp. 1748–1760, 2022.

[33] H. Gao, C. Xiong, J.H. Yin, and H. Deng, Dynamic response and anti-penetration performance of multi-layered heterogeneous composite structure, Acta Mater. Compositae Sin., vol. 36, pp. 228–238, 2019.

[34] Wang Lili, Foundation of Stress Wave, National Defense Industry Press, Beijing, 2005.

[35] Y. Li, K.T. Ramesh, and E.S.C. Chin, The compressive viscoplastic response of an A359/SiCp metal–matrix composite and of the A359 aluminum alloy matrix, Int. J. Solids Struct., vol. 37, no. 51, pp. 7547–7562, 2000. DOI: 10.1016/S0020-7683(99)00304-2.

[36] Y. Li, K. Ramesh, and E. Chin, Dynamic characterization of layered and graded structures under impulsive loading, Int. J. Solids Struct., vol. 38, no. 34–35, pp. 6045–6061, 2001. DOI: 10.1016/S0020-7683(00)00364-4.

[37] J.C.H. Affdl and J.L. Kardos, The Halpin-Tsai equations: A review, Polym. Eng. Sci., vol. 16, no. 5, pp. 344–352, 1976. DOI: 10.1002/pen.760160512.

[38] K.S. Ravichandran, Elastic properties of two-phase composites, J. Am. Ceramic Soc., vol. 77, no. 5, pp. 1178–1184, 1994. DOI: 10.1111/j.1151-2916.1994.tb05390.x.

[39] N. Katsube, Estimation of effective elastic moduli for composites, Int. J. Solids Struct., vol. 32, no. 1, pp. 79–88, 1995. DOI: 10.1016/0020-7683(94)00082-8.

[40] Y. Benveniste, A new approach to the application of Mori-Tanaka's theory in composite materials, Mech. Mater., vol. 6, pp. 147–157, 1987.

[41] Y. Li, H. Zhou, F. Xu, and W. Guo, Effect of gradient distribution of the composition on dynamic response of functionally gradient composites plates under impulsive load, Acta Mater. Compositae Sin., vol. 22, pp. 58–67, 2005.

[42] D.S. Cronin, K. Bui, C. Kaufmann, G. Mclntosh, and T. Berstad, Implementation and validation of the Johnson-Holmquist ceramic material model in LS-Dyna, Proceedings of 4th European LS-DYNA Users Conference, pp. 47–60, 2003.

[43] J.O. Hallquist, LS-DYNA Keyword User's Manual, Livermore Software Technology Corporation, California, pp. 299–800, 2007.

[44] J.O. Hallquist, LS-DYNA Theory Manual, Livermore Software Technology Corporation, California, pp. 25–31, 2006.

[45] H.A. Bruck, A one-dimensional model for designing functionally graded materials to manage stress waves, Int. J. Solids Struct., vol. 37, no. 44, pp. 6383–6395, 2000. DOI: 10.1016/S0020-7683(99)00236-X.

[46] Z.L. Chao, L.T. Jiang, G.Q. Chen, J. Qiao, Q. Z, Z.H. Yu, Y.F. Cao, and G.H. Wu, The microstructure and ballistic performance of B4C/AA2024 functionally graded composites with wide range B4C volume fraction, Compos. Part B., vol. 161, pp. 627–638, 2019. DOI: 10.1016/j.compositesb.2018.12.147.